Proceedings of the KSUPS

Local Structure of Mn in $(La_{1-x}Ho_x)_{2/3}Ca_{1/3}MnO_3$ Studied by X-ray Absorption Fine Structure

A. Pietnoczka[a,*], M. Pękała[b], R. Bacewicz[a], V. Drozd[c], J.F. Fagnard[d], P. Vanderbemden[d], J. Antonowicz[a] and W. Zalewski[a]

[a]Faculty of Physics, Warsaw University of Technology, Koszykowa 75, 00-662 Warsaw, Poland

[b]Department of Chemistry, University of Warsaw, al. Żwirki i Wigury 101, 02-089 Warsaw, Poland

[c]Center for Study Matter at Extreme Conditions, Florida International University, Miami, USA

[d]Montefiore Electricity Institute, University of Liege, 4000 Liege, Belgium

Results of X-ray absorption fine structure measurements in manganites $(La_{1-x}Ho_x)_{2/3}Ca_{1/3}MnO_3$ with $0.15 < x < 0.50$ are presented. When $LaMnO_3$ is doped with a divalent element such as Ca^{2+}, substituting for La^{3+}, holes are induced in the filled Mn d orbitals. This leads to a strong ferromagnetic coupling between Mn sites. Ca ions in $La_{1-x}Ca_xMnO_3$ introduce a distortion of the crystal lattice and mixed valence Mn ions (Mn^{3+} and Mn^{4+}). On the other hand, in manganites $(La_{1-x}Ho_x)_{2/3}Ca_{1/3}MnO_3$ the substitution of La for Ho causes a lattice distortion and induces a disorder, which reduces a magnetic interaction. The ferromagnetic transition temperature and conductivity decrease very quickly with increasing x. The magnetic and transport properties of compounds depend on the local atomic structure around Mn ions. The information on the bond lengths and Debye–Waller factor are obtained from the extended X-ray absorption fine structure (EXAFS) data analysis. The charge state of Mn is determined from the position of the absorption edge in X-ray absorption near edge structure (XANES) data. XAFS results are in good agreement with magnetic characteristics of the studied materials.

PACS numbers: 61.05.cj, 75.47.Lx, 87.64.kd

1. Introduction

Manganese perovskite-based oxides have attracted a renewed interest due to their unusual colossal magnetoresistance (CMR) [1]. They exhibit a great variety of magnetic and transport properties that strongly depend on the stoichiometry and the structure of the materials [2–4].

The $La_{1-x}Ca_xMnO_3$ is one of the most thoroughly studied manganites. The pure compounds like $LaMnO_3$ and $CaMnO_3$ are antiferromagnetic insulators. When $LaMnO_3$ is doped with a divalent element such as Ca^{2+}, substituting for La^{3+}, holes are introduced in the filled Mn d orbitals, which leads to a strong ferromagnetic coupling between Mn sites. Ca ions in $La_{1-x}Ca_xMnO_3$ introduce crystal lattice distortion and mixed valence Mn ions (Mn^{3+} and Mn^{4+}). Compounds in the composition range $0.2 < x < 0.5$ show both ferromagnetic and metallic behaviour, together with the colossal magnetoresistance effect near the Curie temperature T_c. The highest value of $T_c = 270$ K has been obtained for $La_{2/3}Ca_{1/3}MnO_3$ [3]. X-ray absorption fine structure (XAFS) studies of the manganites $La_{1-x}Ca_xMnO_3$ have been reported in a number of papers [5–7].

Mixed-valence manganites $(La_{1-x}RE_x)_{2/3}Ca_{1/3}MnO_3$, where RE = Gd [8, 9], Dy [10, 11], Tb [4], Y [9, 12] were studied. The heavy rare earth elements substitution of La in $(La_{1-x}RE_x)_{2/3}Ca_{1/3}MnO_3$ causes a lattice distortion and introduces an disorder, which reduces the magnetic interaction. The ferromagnetic transition temperature and conductivity decrease very quickly with increasing x. In this study we present results of XAFS measurements in manganites $(La_{1-x}Ho_x)_{2/3}Ca_{1/3}MnO_3$ with $0.15 < x < 0.50$. The present paper is aimed at determination of local atomic structure around Mn ions.

2. Experimental

Polycrystalline $La_{2/3-x}Ho_xCa_{1/3}MnO_3$ samples with $x = 0$, 0.167, 0.333, 0.500, and 0.667 were prepared by citrate sol-gel method [13]. Stoichiometric amounts of high purity $CaCO_3$, La_2O_3 Ho_2O_3 and MnO were dissolved in nitric acid. Citric acid (CA) and ethylene glycol (EG) were added to the solution of metal nitrates in the molar ratio metals:CA:EG = 1:5:5. The resultant solution was evaporated on a water bath at *ca.* 90 °C until a viscous gel-like product was formed. The gels were decomposed by slow heating in air up to 400 °C. The final products were obtained by the heating of decomposed citrate precursor at 1300 °C in air for 24 h.

X-ray powder diffraction was done in transmission geometry using Bruker GADDS/D8 X-ray system with Apex Smart CCD Detector and direct-drive rotating anode. The MacSci rotating anode (Molybdenum) oper-

* corresponding author; e-mail: pietnoczka@if.pw.edu.pl

ates with a 50 kV generator and 20 mA current. X-ray diffraction patterns confirm that samples are single phase and orthorhombic at room temperature. Table I lists the structural data for samples used in this study. For the holmium containing samples the values of unit cell were obtained from XRD data analysis, the data for $LaMnO_3$ and $CaMnO_3$ were taken from Refs. [14, 15]

Manganese K-edge absorption has been measured by the transmission method at HASYLAB synchrotron facility in Hamburg (E4 beamline). The samples were kept at the temperature of 80 K in order to minimize the thermal disorder

The DC magnetization and AC magnetic susceptibility measurements were done by ppms magnetometer equipped with a superconducting coil in the temperature range from 4.2 K to 300 K, in order to determine the magnetic phase diagram.

3. Results and discussion

3.1. XANES

Figure 1 presents the normalized XANES spectra at the K-edge of Mn for the samples used in this study. The plots illustrating the data series were vertically shifted for clarity. The general shape of the spectra is very similar to each other, thus introduction of holmium does not cause any significant changes in the electronic structure The XANES spectrum for $CaMnO_3$ has a few specific features which differ from those of $LaMnO_3$ (Fig. 1). Only the $CaMnO_3$ spectrum has a pre-peak (labeled as A in Fig. 1), the second oscillation has a different shape and a maximum at higher energy (labeled as B in Fig. 1) and the second minimum is for higher energy (labeled as C in Fig. 1). Considering these differences the XANES spectra for the higher holmium concentration (Ho23 and Ho12) are similar to that of $CaMnO_3$, and the spectra of the next two samples (Ho13 and Ho16) bear closer resemblance to that of $LaMnO_3$ Ho atoms have the lower ionic radius than La atoms like Ca atoms. Hence, the higher concentration of holmium shrinks the unit cell and XANES spectra for those samples become similar to those of $CaMnO_3$ (Table I).

The charge state of Mn can be determined from the position of the absorption edge. In $La_{1-x}Ca_xMnO_3$ manganites, systematic shifts in the absorption edge position of the Mn K-edge with a changing of composition have been reported [6, 7]. In our case the position of the absorption edge is approximately constant throughout the series (Fig. 2). This means that the ratio of Mn^{3+} to Mn^{4+} is constant. In Fig. 2 the $LaMnO_3$ and $CaMnO_3$ compounds were used as reference data for the Mn^{3+} and Mn^{4+}, respectively.

3.2. EXAFS

Theoretical EXAFS spectra were calculated using a real-space multiple-scattering approach represented by the FEFF8 code [16]. Structural data of $LaMnO_3$ (the space group *Pnma*, a = 5.4910 Å, b = 7.77640 Å, c = 5.53230 Å [14]) and $CaMnO_3$ (the space group *Pnma*, a = 5.28160 Å, b = 7.45670 Å, c = 5.26710 Å [15]) were used. We used a cluster with a radius of 10 Å containing 410 atoms. The EXAFS data were extracted from the raw absorption data with the ATHENA program, and non-linear fitting was carried out using the ARTHEMIS program (both programs from the IFEFFIT package [17, 18]).

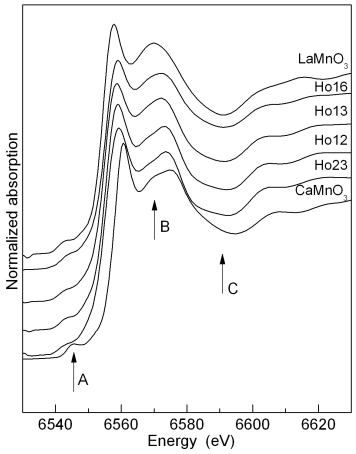

Fig. 1. Normalized XANES data at the Mn K-edge. The graphs are vertically shifted for clarity.

TABLE I

The structural data for the samples used in the study.

Name	Composition	a [Å]	b [Å]	c [Å]
$LaMnO_3$	$LaMnO_3$	5.4910	7.7764	5.5323
Ho16	$La_{1/2}Ho_{1/6}Ca_{1/3}MnO_3$	5.4372	7.6754	5.4637
Ho13	$La_{1/3}Ho_{1/3}Ca_{1/3}MnO_3$	5.4052	7.6233	5.4653
Ho12	$La_{1/6}Ho_{1/2}Ca_{1/3}MnO_3$	5.3547	7.5530	5.4944
Ho23	$La_{1/6}Ho_{1/2}Ca_{1/3}MnO_3$	5.2857	7.4664	5.5388
$CaMnO_3$	$CaMnO_3$	5.2816	7.4567	5.2671

Figure 3 presents EXAFS functions for all manganites used in this study. Fourier transforms were made in the k-range from 3 $Å^{-1}$ to 10 $Å^{-1}$ and the fits were made in the 1.0–4.2 Å range, i.e., within three coordination shells. The best fit parameters for the $LaMnO_3$ model are listed in Table II. It contains the first shell parameters Mn–O distance (column $R_{Mn–O}$), mean-square displacement (Debye–Waller factor, σ_1^2) and analogically the second shell parameters assumed that X could be La or Ho, or Ca atom. The EXAFS is known to be not sensitive to relative contents of specific elements in the second coordination shell due to negligible differences in the photoelectron scattering phases. Table II contains also the values of the R-factor revealing a quality of the fit [18]. The first shell is composed of three sub-shells with differences in distances between them not exceeding 0.004 Å. Therefore, we used a single value $R_{Mn–O}$

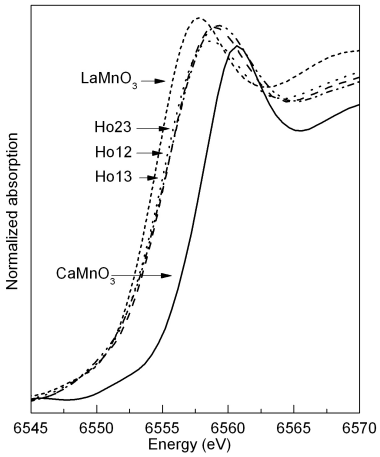

Fig. 2. The main absorption edge for $(La_{1-x}Ho_x)_{2/3}Ca_{1/3}MnO_3$ series. The $LaMnO_3$ and $CaMnO_3$ were used as references.

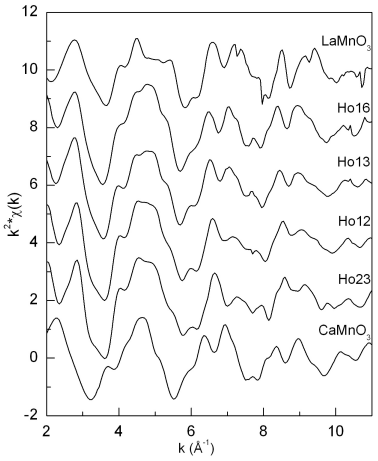

Fig. 3. EXAFS functions (multiplied by k^2) for manganites used in the study.

in the fit like for the second shell which is composed of four sub-shells with differences in distances not greater than 0.17 Å. We assumed the coordination numbers N as fixed and equal to $LaMnO_3$ values for all the coordination shells. We also set the passive electron amplitude reduction factor S_0^2 to be 075 in all the fits. This value was obtained from the fit to $LaMnO_3$ data. Multiple scattering paths were included (35 paths in total). We tried to fit with the $CaMnO_3$ model but in all cases less satisfactory fits were obtained (higher R-factor values). We fitted also a mixture of $LaMnO_3$ and $CaMnO_3$ models with the relative concentration of both sites fixed as 0.66. For all the samples we obtained a smaller R-factor, but a higher reduced chi-square values [18], which means that the better fit was achieved only because of more fitting parameters introduced to the fit.

Figure 4 presents a comparison of the experimental data for the Ho13 sample and fitted EXAFS plots for

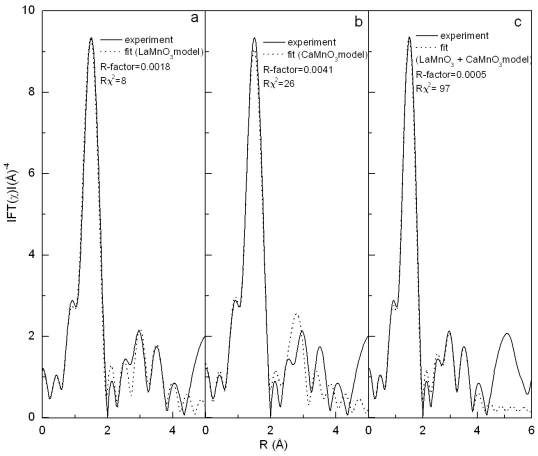

Fig. 4. Experimental (solid lines) and fitted (dotted lines) EXAFS plots for the Ho13 sample with the model of: (a) $LaMnO_3$, (b) $CaMnO_3$ and (c) mixture of $LaMnO_3$ and $CaMnO_3$.

$LaMnO_3$ (Fig. 4a), $CaMnO_3$ (Fig. 4b) and mixture of $LaMnO_3$ and $CaMnO_3$ (Fig. 4c) models. It should be underlined, that the discrimination between these three models is based on the EXAFS spectra from the second coordination shell, which contains 8 La atoms in $LaMnO_3$ and 8 Ca atoms in $CaMnO_3$. In the case of $(La_{1-x}Ho_x)_{2/3}Ca_{1/3}MnO_3$ some of the lanthanum atoms within the second coordination shell, were replaced with holmium and calcium atoms. The $LaMnO_3$ model was proved to be better for all the samples because the photoelectron scattering phase and amplitude plots for La and Ho are similar to each other (Fig. 5a,b) and in the measured series the content ratio (La + Ho) to Ca is equal to 2:1. Figure 6 presents the best fitting with $LaMnO_3$ model for the other $(La_{1-x}Ho_x)_{2/3}Ca_{1/3}MnO_3$ samples (Ho16, Ho12, Ho23).

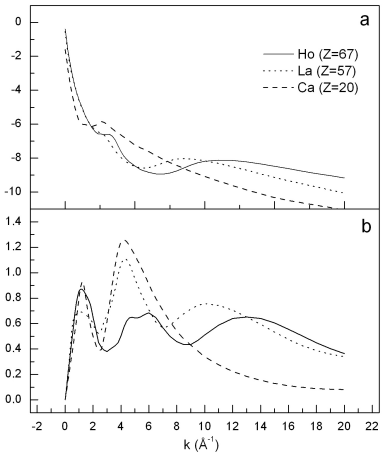

Fig. 5. Comparison of scattering phases (a) and scattering amplitudes (b) for La, Ho and Ca atoms.

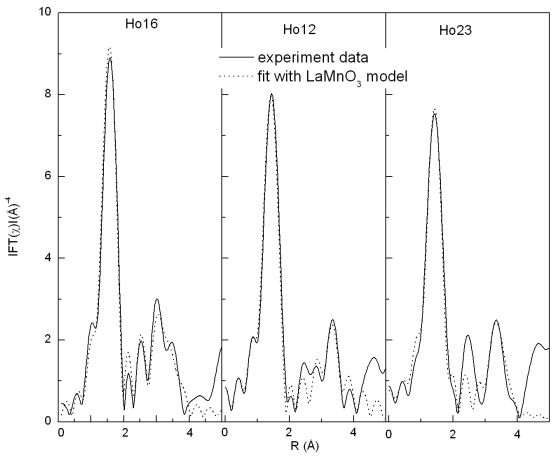

Fig. 6. EXAFS plots — experimental (solid lines) and fitted (dotted lines) with the use of $LaMnO_3$ model.

The fitting results indicate decreasing distances between atoms and increasing Debye–Waller factors with the increasing Ho concentration. The bond length is decreased due to the lower ionic radius of holmium (Table II). Smaller Mn–O distances cause the Mn–O–Mn bond angle to be smaller than 180°. The Mn–O–Mn angle is known to determine the magnetic and transport properties in manganites compounds [19]. Additionally, the structural disorder increases versus the concentration of Ho (Table II). The less satisfactory fit was achieved for Ho23 sample, when all La atoms were substituted for Ho atoms and the second coordination shell had the lowest amplitude, which is correlated with the highest Debye–Waller factor.

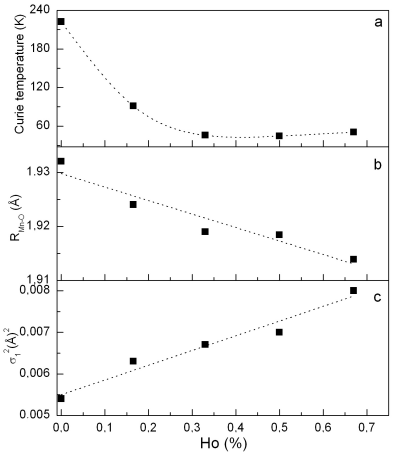

Fig. 7. The Curie temperature (a), $R_{\mathrm{Mn–O}}$ distance (b) and Debye–Waller factor σ_1^2 (c) as a function of Ho content.

TABLE II

Fitting parameters for the $LaMnO_3$ model. The values fixed during the fitting are bolded.

Sample	N	$R_{\mathrm{Mn–O}}$ [Å]	σ_1^2 [Å^2]	N	$R_{\mathrm{Mn–X}}$ [Å]	σ_2^2 [Å^2]	R-factor
La MnO_3	**6**	1.932	0.0054	**8**	3.334	0.0063	0.0005
$La_{1/2}Ho_{1/6}Ca_{1/3}MnO_3$	**6**	1.924	0.0063	**8**	3.330	0.00782	0.0018
$La_{1/6}Ho_{1/2}Ca_{1/3}MnO_3$	**6**	1.919	0.0067	**8**	3.329	0.00814	0.0018
$La_{1/3}Ho_{1/3}Ca_{1/3}MnO_3$	**6**	1.917	0.0070	**8**	3.317	0.01051	0.0040
$Ho_{2/3}Ca_{1/3}MnO_3$	**6**	1.914	0.0080	**8**	3.303	0.01312	0.0100
Error	–	±0.010	±0.0005	–	±0.050	±0.0010	–

In Fig. 7 structural parameters for the first coordination shell, obtained from fitting, and the Curie temperature are compared against the Ho concentration. Our results show that the substitution for La with Ho induces a decreasing of Mn–O distances and an increasing of Debye–Waller factors. Also, the Mn–O–Mn bond angles decrease, which leads to weakening of the double exchange interaction and corresponds to decrease of the Curie temperature with increasing Ho content. The same conclusions were obtained in the cases, where the effect of substituting La for rare earth elements causes an increase of the orthorhombic distortion of the lattice, which leads to the decrease of the metal-insulator transition temperature [4, 8–12].

4. Conclusions

We investigated the local order around Mn ions in manganites $(La_{1-x}Ho_x)_{2/3}Ca_{1/3}MnO_3$ in the composition range $0.15 < x < 0.50$. The general shape of XANES spectra is very similar for all the samples used in this study, thus introduction of holmium does not cause any significant changes in the electronic structure The same value of the shift in the absorption edge position of the

Mn K-edge point to the same ratio of Mn^{4+} and Mn^{3+} ions in all the samples containing holmium.

The substitution of La for Ho lowers the Curie temperature. The plausible reason for this is the change in the local structure around the Mn atom. The EXAFS analysis indicates that for an increasing holmium concentration, the Debye–Waller factors increase and the bond lengths decrease. Smaller Mn–O distances cause a decrease of the Mn–O–Mn bond angle, which leads to the decrease of the Curie temperature with increasing Ho content.

Acknowledgments

This study was partially supported by Ministry of Science and Higher Education (PL) and CGRI (BE) within the Scientific Cooperation Wallony &#8211. Poland and the research leading to these results have received funding from the European Community's Seventh Framework Programme (FP7/2007-2013) under grant agreement no. 226716. The authors would like to thank Dr Dariusz Zając from HASYLAB for the experimental assistance.

References

[1] B. Salamon, M. Jaime, *Rev. Mod. Phys.* **73**, 583 (2001).

[2] C.H. Booth, F. Bridges, G.H. Kwei, J.M. Lawrence, A.L. Cornelius, J.J. Neumeier, *Phys. Rev. B* **57**, 10440 (1998).

[3] G. Subias, J. Garcia, J. Blasco, M. Conception-Sanchez, M. Grazia-Proietti, *J. Phys., Condens. Matter* **14**, 5017 (2002).

[4] J. Blasco, J. Garcia, J.M. de Teresa, M.R. Ibarra, P.A. Algarabel, C. Marquina, *J. Phys., Condens. Matter* **8**, 7427 (1996).

[5] J. Garcia, M. Conception-Sanchez, G. Subias, J. Blasco, *J. Phys., Condens. Matter* **13**, 3229 (2001).

[6] M. Sikora, C. Kapusta, K. Knžek, Z. Jirák, C. Autret, M. Borowiec, C.J. Oates, V. Procházka, D. Rybicki, D. Zając, *Phys. Rev. B* **73**, 094426 (2006).

[7] G. Subias, J. Garcia, M.G. Proietti, J. Blasco, *Phys. Rev. B* **56**, 8183 (1997).

[8] M. Pękała, V. Drozd, J. Kovac, I. Skorvanek, *Czechosl. J. Phys.* **54**, D415 (2004).

[9] D. Uthra, *Bulg. J. Phys.* **35**, 125 (2008).

[10] S.M. Yusuf, R. Ganguly, K.R. Chakraborty, P.K. Mishra, S.K. Paranjpe, J.V. Yakhmi, V.C. Sahni, *J. Alloys. Compd.* **326**, 89 (2001).

[11] V. Drozd, M. Pękała, J. Kovac, I. Skorvanek, S. Nedilko, *Acta Phys. Pol. A* **106**, 751 (2004).

[12] S. Jin, H.M. O'Bryan, T. Tiefel, M. Mc Cormack, W.W. Rhodes, *Appl. Phys. Lett.* **66**, 382 (1995).

[13] M. Gaudon, C.L. Robert, F. Ansart, P. Stevens, A. Rousset, *Sol. Stat. Sci.* **4**, 125 (2002).

[14] V.A. Cherpanov, E.A. Filonova, V.I. Voronin, I.F. Berger, *J. Sol. Stat. Chem.* **153**, 205 (2000).

[15] E.S. Božin, A. Sartbaeva, H. Zheng, S.A. Wells, J.F. Mitchell, Th. Proffen, M.F. Thorpe, S.J.L. Billinge, *J. Phys. Chem. Sol.* **69**, 2146 (2008).

[16] A.L. Ankundinov, B. Ravel, J.J. Rehr, S.D. Conradson, *Phys. Rev. B* **58**, 756 (1998).

[17] M. Newville, B. Ravel, D. Haskel, J.J. Rehr, E.A. Stern, Y. Yacoby, *Physica B* **208/209**, 154 (1995).

[18] E.A. Stern, M. Newville, B. Ravel, Y. Yacoby, D. Haskel, *Physica B* **208/209**, 117 (1995).

[19] H.Y. Hwang, S.-W. Cheong, P.G. Radaelli, M. Marezio, B. Batlogg, *Phys. Rev. Lett.* **75** 914 (1995).